

# The Statistics of Weak Lensing at Small Angular Scales: Probability Distribution Function

Dipak Munshi<sup>1</sup> and Bhuvnesh Jain<sup>2</sup>

<sup>1</sup>*Max-Planck-Institut für Astrophysik, Karl-Schwarzschild-Str.1, D-85740, Garching, Germany*

<sup>2</sup>*Johns Hopkins University, Department of Physics, Baltimore, MD 21218, USA*

29 April 2024

## ABSTRACT

Weak gravitational lensing surveys have the potential to directly probe mass density fluctuation in the universe. Recent studies have shown that it is possible to model the statistics of the convergence field at small angular scales by modeling the statistics of the underlying density field in the highly nonlinear regime. We propose a new method to model the complete probability distribution function of the convergence field as a function of smoothing angle and source redshift. The model relies on a hierarchical ansatz for the behavior of higher order correlations of the density field. We compare our results with ray tracing simulations and find very good agreement over a range of smoothing angles. Whereas the density probability distribution function is not sensitive to the cosmological model, the probability distribution function for the convergence can be used to constrain both the power spectrum and cosmological parameters.

**Key words:** Cosmology: theory – large-scale structure of the Universe – Methods: analytical

## 1 INTRODUCTION

Weak distortions in the images of high red-shift galaxies by the intervening large-scale structure provide us with valuable information about the mass distribution in the universe. The study of such distortions provides us a unique way to probe the statistical properties of the intervening density distribution. Traditionally, the study of gravitational clustering in the quasi-linear and non-linear regime are done by analyzing galaxy catalogs. However such studies can only provide us with information on how the galaxies are clustered, and to infer the statistics of the underlying mass distribution from galaxy catalogs one needs a prescription for galaxy bias. Weak lensing studies are free from such effects and can directly probe the statistics of the underlying mass distribution.

Pioneering works in this direction were done by Blandford et al. (1991), Miralda-Escude (1991) and Kaiser (1992) based on the earlier work by Gunn (1967). Current progress in weak lensing can broadly be divided into two distinct categories. Whereas Villumsen (1996), Stebbins (1996), Bernardeau et al. (1997), Jain & Seljak (1997) and Kaiser (1998) have focussed on the linear and quasi-linear regime by assuming a large smoothing angle, several authors have developed a numerical technique to simulate weak lensing catalogs. Numerical simulations of weak lensing typically employ N-body simulations, through which ray tracing experiments are conducted (Schneider & Weiss 1988; Jarosszn’ski et al. 1990; Lee & Paczyn’ski 1990; Jarosszn’ski 1991; Babul & Lee 1991; Bartelmann & Schneider 1991, Blandford et al. 1991). Building on the earlier work of Wambsganns et al. (1995, 1997, 1998) detailed numerical study of lensing was done by Wambsganns, Cen & Ostriker (1998). Other recent studies using ray tracing experiments have been conducted by Premadi, Martel & Matzner (1998), van Waerbeke, Bernardeau & Mellier (1998), Bartelmann et al (1998), Couchman, Barber & Thomas (1998) and White & Hu (1999). While a perturbative analysis can provide valuable information at large smoothing angles, it can not be used to study lensing at small angular scales as the whole perturbative series starts to diverge.

A complete analysis of weak lensing statistics at small angular scales is not available at present, as we do not have a similar analysis for the underlying dark matter distribution. However there are several non-linear *ansatze* which predicts a tree hierarchy for matter correlation functions and are thought to be successful to some degree in modeling results from numerical simulations. Most of these *ansatze* assumes a tree hierarchy for higher order correlation functions and they disagree with each other by the way they assign weights to trees of same order but of different topologies (Balian & Schaeffer 1989, Bernardeau & Schaeffer 1992; Szapudi & Szalay). The evolution of the two-point correlation functions in all such approximations are left arbitrary. However recent studies by several authors (Hamilton et al 1991; Peacock & Dodds 1994; Nityanada & Padmanabhan 1994; Jain, Mo & White 1995; Peacock & Dodds 1996) have provided us accurate fitting formulae for the evolution of the

two-point correlation function, which can be used in combination with these hierarchical *ansatze* to predict the clustering properties of dark matter distribution in the universe.

Most recent studies in weak lensing have mainly focussed on lower order cumulants (van Waerbeke, Bernardeau & Mellier 1998; Schneider et al 1998; Hui 1999; Munshi, Jain & White 1999a), cumulant correlators (Munshi, Jain & White 1999a) and errors associated with their measurement from observational data using different filter functions (Reblinsky et al. 1999). However it is well known that higher order moments are increasingly sensitive to the tail of the distribution function and are more sensitive to measurement errors due to the finite size of a catalog. On the other hand numerical simulations involving ray tracing experiments have already shown that while the probability distribution function associated with the density field is not sensitive to cosmological parameters, its weak lensing counterpart can help us in the estimation of such parameters from observational data (Jain, Seljak & White 1999). At present there is no prescription for the theoretical estimation of the PDF for the smoothed convergence field  $\kappa(\theta_0)$ . Valageas (1999) has used a hierarchical ansatz for computing the error involved in the estimation of  $\Omega_0$  and  $\Lambda$  from SNeIa observations. A similar fitting function was recently proposed by Wang (1999). Our formalism is similar to that of Valageas (1999) although the results obtained by us include the effect of smoothing. The formalism we introduce can be easily extended to the multi-point PDF and hence to compute bias and  $S_N$  parameters associated with “hot spots” of convergence maps. Analytical results and detailed comparison against numerical simulations will be presented elsewhere.

The paper is organized as follows. In section 2 we briefly the ray tracing simulations. Section 3 presents the analytical results necessary to compute the PDF of the smoothed convergence field  $\kappa(\theta_0)$ . The comparison of these results with ray tracing simulations is made in section 4. Section 5 contains a discussion of our results.

## 2 GENERATION OF CONVERGENCE MAPS FROM N-BODY SIMULATIONS

Convergence maps are generated by solving the geodesic equations for the propagation of light rays through N-body simulations of dark matter clustering. The simulations used for our study are adaptive  $P^3M$  simulations with  $256^3$  particles and were carried out using codes kindly made available by the VIRGO consortium. These simulations can resolve structures larger than  $30h^{-1}kpc$  at  $z = 0$  accurately. These simulations were carried out using 128 or 256 processors on CRAY T3D machines at Edinburgh Parallel Computer Center and at the Garching Computer Center of the Max-Planck Society. These simulations were intended primarily for studies of the formation and clustering of galaxies (Kauffmann et al 1999a, 1999b; Diaferio et al 1999) but were made available by these authors and by the Virgo Consortium for this and earlier studies of gravitational lensing (Jain, Seljak & White 1999, Reblinsky et al. 1999, Munshi & Jain 1999a)

Ray tracing simulations were carried out by Jain et al. (1999) using a multiple lens-plane calculation which implements the discrete version of recursion relations for mapping the photon position and the Jacobian matrix (Schneider & Weiss 1988; Schneider, Ehler & Falco 1992). In a typical experiment  $4 \times 10^6$  rays are used to trace the underlying mass distribution. The dark matter distribution between the source and the observer is projected onto 20 - 30 planes. The particle positions on each plane are interpolated onto a  $2048^2$  grid. On each plane the shear matrix is computed on this grid from the projected density by using Fourier space relations between the two. The photons are propagated starting from a rectangular grid on the first lens plane. The regular grid of photon position gets distorted along the line of sight. To ensure that all photons reach the observer, the ray tracing experiments are generally done backward in time from the observer to the source plane at red-shift  $z = z_s$ . The resolution of the convergence maps is limited by both the resolution scale associated with numerical simulations and also due to the finite resolution of the grid to propagate photons. The outcome of these simulations are shear and convergence maps on a two dimensional grid. Depending on the background cosmology the two dimensional box represents a few degree scale patch on the sky. For more details on the generation of  $\kappa$ -maps, see Jain et al (1999).

## 3 ANALYTICAL PREDICTIONS

In this section we provide the necessary theoretical background for the analytical derivation of the probability distribution function for the smoothed convergence field  $\kappa(\theta_0)$ . We will use models of nonlinear hierarchical clustering; details of various hierarchical ansatzes can be found in Balian & Schaeffer (1989), Bernardeau & Schaeffer (1992,1999), Bernardeau (1992,1994), Szapudi & Szalay (1993), Munshi et al. (1999a,b,c), Valageas & Schaeffer (1998), Valageas et al. (1997).

The following line element describes the background geometry of the universe:

$$d\tau^2 = -c^2 dt^2 + a^2(t)(d\chi^2 + r^2(\chi)d^2\Omega) \quad (1)$$

Where we have denoted the angular diameter distance by  $r(\chi)$  and scale factor of the universe by  $a(t)$ ;  $r(\chi) = K^{-1/2} \sin(K^{-1/2}\chi)$  for positive curvature,  $r(\chi) = (-K)^{-1/2} \sinh((-K)^{-1/2}\chi)$  for negative curvature and  $r(\chi) = \chi$  for a zero curvature universe. The curvature  $K$  is given in terms of the present value  $H_0$  and  $\Omega_0$  as  $K = (\Omega_0 - 1)H_0^2$ . Parameters characterising different cosmological models that we will be studying are listed in Table 1.

**Table 1.** Cosmological parameters characterizing different models

	SCDM	TCDM	LCDM	OCDM
$\Gamma$	0.5	0.21	0.21	0.21
$\Omega_0$	1.0	1.0	0.3	0.3
$\Lambda_0$	0.0	0.0	0.7	0.0
$\sigma_8$	0.6	0.6	0.9	0.85
$H_0$	50	50	70	70

### 3.1 Formalism

The statistics of the convergence  $\kappa$  in weak lensing is very similar to that of the projected density. In our analysis we will consider a small patch of the sky where we can use the plane parallel approximation or small angle approximation to replace spherical harmonics by Fourier modes. The 3-dimensional density contrast  $\delta$  along the line of sight when projected onto the sky with the weight function  $\omega(\chi)$  gives the convergence in a direction  $\gamma$ .

$$\kappa(\gamma) = \int_0^{\chi_s} d\chi \omega(\chi) \delta(r(\chi)\gamma) \quad (2)$$

In our discussion we will assume the source galaxies to be at a fixed red-shift  $z_s$ . For this case, one can express the weight function as,

$$\omega(\chi) = \frac{3}{4} \frac{H_0^2}{c^2} \Omega_m a \frac{r(\chi)r(\chi_s - \chi)}{r(\chi_s)}, \quad (3)$$

where  $\chi_s$  is the comoving radial distance to the source galaxies. Using the Fourier transform of  $\delta$ , the convergence can be expressed as:

$$\kappa(\gamma) = \int_0^{\chi_s} d\chi \omega(\chi) \int \frac{d^3\mathbf{k}}{(2\pi)^3} \exp(i\chi k_{\parallel} + ir\theta k_{\perp}) \delta_{\mathbf{k}}, \quad (4)$$

where  $\theta$  denotes the angle between the line of sight direction  $\gamma$  and the wave vector  $\mathbf{k}$ ,  $k_{\parallel}$  and  $k_{\perp}$  denote the components of  $\mathbf{k}$ , parallel and perpendicular to the line of sight. In the small angle approximation one assumes that  $k_{\perp} \gg k_{\parallel}$ . Using these definitions we can compute the projected two-point correlation function in terms of the dark matter power spectrum  $P(k, \chi)$  (Peebles 1980, Kaiser 1992, Kaiser 1998):

$$\langle \kappa(\gamma_1) \kappa(\gamma_2) \rangle = \int_0^{\chi_s} d\chi \frac{\omega^2(\chi)}{r^2(\chi)} \int \frac{d^2\mathbf{l}}{(2\pi)^2} \exp(i\theta l) P\left(\frac{l}{r(\chi)}, \chi\right). \quad (5)$$

Where we have introduced  $\mathbf{l} = r(\chi)\mathbf{k}_{\perp}$  to denote the scaled wave vector projected on the sky. The variance of  $\kappa$  smoothed over an angle  $\theta_0$  is (Jain & Seljak 1997)

$$\langle \kappa^2(\theta_0) \rangle = \int_0^{\chi_s} d\chi_1 \frac{\omega^2(\chi_1)}{r^2(\chi_1)} \int \frac{d^2\mathbf{l}}{(2\pi)^2} P\left(\frac{l}{r(\chi)}, \chi\right) W_2^2(l\theta_0) \quad (6)$$

Similarly the higher order moments of the smoothed convergence field relate  $\langle \kappa^P(\theta_0) \rangle$  to the 3-dimensional multi-spectra of the underlying dark matter distribution  $B_p$  (Hui 1999, Munshi & Coles 1999a):

$$\langle \kappa^3(\theta_0) \rangle = \int_0^{\chi_s} d\chi_1 \frac{\omega^3(\chi)}{r^6(\chi)} \int \frac{d^2\mathbf{l}_1}{(2\pi)^3} W_2(l_1\theta_0) \int \frac{d^2\mathbf{l}_2}{(2\pi)^2} W_2(l_2\theta_0) \int \frac{d^2\mathbf{l}_3}{(2\pi)^3} W_2(l_3\theta_0) B_3\left(\frac{l_1}{r(\chi)}, \frac{l_2}{r(\chi)}, \frac{l_3}{r(\chi)}, \chi\right) \sum_{\mathbf{l}_i=0} \quad (7)$$

$$\langle \kappa^4(\theta_0) \rangle = \int_0^{\chi_s} d\chi_1 \frac{\omega^4(\chi)}{r^8(\chi)} \int \frac{d^2\mathbf{l}_1}{(2\pi)^3} W_2(l_1\theta_0) \int \frac{d^2\mathbf{l}_2}{(2\pi)^2} W_2(l_2\theta_0) \int \frac{d^2\mathbf{l}_3}{(2\pi)^2} W_2(l_3\theta_0) \int \frac{d^2\mathbf{l}_4}{2\pi^2} W_2(l_4\theta_0) \quad (8)$$

$$B_4\left(\frac{l_1}{r(\chi)}, \frac{l_2}{r(\chi)}, \frac{l_3}{r(\chi)}, \frac{l_4}{r(\chi)}, \chi\right) \sum_{\mathbf{l}_i=0}.$$

We will use these results to show that it is possible to compute the complete probability distribution function of  $\kappa$  from the underlying dark matter probability distribution function. Details of the analytical results presented here can be found in Munshi & Coles (1999b).

### 3.2 Hierarchical Ansatz

The spatial length scales corresponding to small angles are in the highly non-linear regime. Assuming a tree model for the matter correlation hierarchy in the highly non-linear regime, one can write the general form of the  $N$ th order correlation function as (Groth & Peebles 1977, Fry & Peebles 1978, Davis & Peebles 1983, Bernardeau & Schaeffer 1992, Szapudi & Szalay 1993):

$$\xi_N(\mathbf{r}_1, \dots, \mathbf{r}_N) = \sum_{\alpha, N\text{-trees}} Q_{N,\alpha} \sum_{\text{labellings}} \prod_{\text{edges}}^{(N-1)} \xi(\mathbf{r}_i, \mathbf{r}_j). \quad (9)$$

It is interesting to note that a similar hierarchy develops in the quasi-linear regime in the limit of vanishing variance (Bernardeau 1992); however the hierarchal amplitudes  $Q_{N,\alpha}$  become shape dependent functions in the quasilinear regime. In the highly nonlinear regime there are some indications that these functions become independent of shape, as suggested by studies of the lowest order parameter  $Q_3 = Q$  using high resolution numerical simulations (Scocimarro et al. 1998). In Fourier space such an ansatz means that the hierarchy of multi-spectra can be written as sums of products of the matter power-spectrum.

$$B_2(\mathbf{k}_1, \mathbf{k}_2, \mathbf{k}_3) \sum_{k_i=0} = Q(P(\mathbf{k}_1)P(\mathbf{k}_2) + P(\mathbf{k}_2)P(\mathbf{k}_3) + P(\mathbf{k}_3)P(\mathbf{k}_1)) \quad (10)$$

$$B_3(\mathbf{k}_1, \mathbf{k}_2, \mathbf{k}_3, \mathbf{k}_4) \sum_{k_i=0} = R_a P(\mathbf{k}_1)P(\mathbf{k}_1 + \mathbf{k}_2)P(\mathbf{k}_1 + \mathbf{k}_2 + \mathbf{k}_3) + \text{cyc.perm.} + R_b P(\mathbf{k}_1)P(\mathbf{k}_2)P(\mathbf{k}_3) + \text{cyc.perm.}$$

Different hierarchical models differ in the way they predict the amplitudes of different tree topologies. Bernardeau & Schaeffer (1992) considered the case where amplitudes in general are factorizable, at each order one has a new “star” amplitude and higher order “snake” and “hybrid” amplitudes can be constructed from lower order “star” amplitudes (see Munshi, Melott & Coles 1999a,b,c for a detailed description). In models proposed by Szapudi & Szalay (1993) it was assumed that all hierarchal amplitudes of any given order are degenerate. Galaxy surveys have been used to study these *ansatze*. Our goal here is to show that weak-lensing surveys can also provide valuable information in this direction, in addition to constraining the matter power-spectra and background geometry of the universe. We will use the model proposed by Bernardeau & Schaeffer (1992) and its generalization to the quasi-linear regime by Bernardeau (1992, 1994) to construct the PDF of the convergence field  $\kappa(\theta_0)$ . We express the one-point cumulants as:

$$\langle \kappa^3(\gamma) \rangle = (3Q_3)\mathcal{C}_3[\kappa_{\theta_0}^2] = S_3 \langle \kappa^2(\theta_0) \rangle^2 \quad (11)$$

$$\langle \kappa^4(\gamma) \rangle = (12R_a + 4R_b)\mathcal{C}_4[\kappa_{\theta_0}^3] = S_4 \langle \kappa^2(\theta_0) \rangle^3, \quad (12)$$

where

$$\mathcal{C}_t[\kappa^m(\theta_0)] = \int_0^{\chi_s} \frac{\omega^t(\chi)}{r^2(t-1)(\chi)} \kappa_{\theta_0}^m d\chi, \quad (13)$$

and

$$\kappa_{\theta_0} = \int \frac{d^2\mathbf{l}}{(2\pi)^2} P\left(\frac{l}{r(\chi)}\right) W_2^2(l\theta_0). \quad (14)$$

Equation (11) was derived by Hui (1998). He showed that his result agrees well with the ray tracing simulations of Jain, Seljak and White (1998). More recent studies have shown that two-point statistics such as cumulant correlators can also be modeled in a similar way (Munshi & Coles 1999, Munshi, Jain & White 1999).

### 3.3 Scaling Models and Generating Functions

The success of analytical results on lower order cumulants, when compared with numerical ray tracing experiments, motivates a more general analysis of the probability distribution function of the smoothed convergence field  $\kappa(\theta_0)$ . For this purpose we found the formalism developed by Balian & Schaeffer (1989) and Bernardeau & Schaeffer (1992) to be most suitable. These results are based on a general tree hierarchy of higher order correlation functions and the assumption that the amplitudes associated with different tree-topologies are constant in the highly non-linear regime. These results were generalized by Bernardeau (1992, 1994) to the quasi-linear regime where the perturbative dynamics can be used to make more concrete predictions. In this section we review the basic results from the scaling models before extending such models to the statistics of the smoothed convergence field  $\kappa(\theta_0)$  (for more details see Munshi & Coles 1999b). We will use the small angle approximation throughout our derivation. Our results can be generalized to the case of the projected clustering of galaxies.

In a scaling analysis of the probability distribution function (PDF), the void probability distribution function (VPF) plays a fundamental role. The VPF can be related to the generating function of the cumulants or  $S_N$  parameters,  $\phi(y)$  (White 1979, Balian & Schaeffer 1989).

$$P_v(0) = \exp(\bar{N}\sigma(N_c)) = \exp\left(-\frac{\phi(N_c)}{\xi_2}\right), \quad (15)$$

where  $P_v(0)$  is the probability of having no “particles” in a cell of volume  $v$ ,  $\bar{N}$  is the average occupancy of the particles and  $N_c = \bar{N}\xi_2$ . The VPF is meaningful only for a discrete distribution of particles and can not be defined for smoothed fields such as  $\delta$  or  $\kappa(\theta_0)$ . However the scaling functions defined above as  $\sigma(y) = -\phi(y)/y$ , are very useful even for continuous distributions where they can be used as a generating function of the one-point cumulants or the  $S_N$  parameters.

$$\phi(y) = \sum_{p=1}^{\infty} \frac{S_p}{p!} y^p \quad (16)$$

The function  $\phi(y)$  satisfies the constraint  $S_1 = S_2 = 1$  necessary for the normalization of the PDF. The other generating function which plays a very important role in such an analysis is the generating function for vertex amplitudes  $\nu_n$ , associated with nodes appearing in the tree representation of the higher order correlation hierarchy ( $Q_3 = \nu_2$ ,  $R_a = \nu_2^2$  and  $R_b = \nu_3$ ).

$$\mathcal{G}(\tau) = 1 - \tau + \frac{\nu_2}{2!} \tau^2 - \frac{\nu_3}{3!} \tau^3 + \dots \quad (17)$$

A more specific model for  $\mathcal{G}(\tau)$  is sometimes used, which is useful in making more detailed predictions (Bernardeau & Schaeffer 1979):

$$\mathcal{G}(\tau) = \left(1 + \frac{\tau}{\kappa_a}\right)^{-\kappa_a} \quad (18)$$

We will relate  $\kappa$  with other parameters of scaling models. While the definition of VPF does not use any specific form of the hierarchical ansatz, writing the tree amplitudes in terms of the weights associated with the nodes is only possible when one assumes a factorizable model for the tree hierarchy (Bernardeau & Schaeffer 1992). Moreover, in such an ansatz the generating functions for the tree nodes can be related to the VPF by solving a pair of implicit equations (Balian & Schaeffer 1989).

$$\phi(y) = y\mathcal{G}(\tau) - \frac{1}{2}y\tau \frac{d}{d\tau}\mathcal{G}(\tau) \quad (19)$$

$$\tau = -y \frac{d}{d\tau}\mathcal{G}(\tau) \quad (20)$$

The VPF and PDF can be related to each other by the following equation (Balian & Schaeffer 1989)

$$P(\delta) = \int_{-i\infty}^{i\infty} \frac{dy}{2\pi i} \exp\left[\frac{(1+\delta)y - \phi(y)}{\xi_2}\right] \quad (21)$$

So it is clear that the properties of  $\phi(y)$  completely determine the behavior of  $P(\delta)$  for all values of  $\delta$ . However different asymptotic expressions of  $\phi(y)$  govern the behaviour of  $P(\delta)$  for different intervals of  $\delta$ . For large  $y$  we can express  $\phi(y)$  as

$$\phi(y) = ay^{1-\omega}. \quad (22)$$

We have introduced a new variable  $\omega$  for the description of VPF. This parameter plays a very important role in the scaling analysis. No theoretical analysis has been done so far to link  $\omega$  with the initial power spectral index  $n$ . Numerical simulations are generally used to fix  $\omega$  for different initial conditions. Such studies have confirmed that an increase of power on smaller scales increases the value of  $\omega$ . Typically an initial power spectrum with spectral index  $n = -2$  (which should model CDM-like spectra that we have considered in our simulations at small length scales) produces a value of  $\omega = 0.3$  which we will use in our analysis of the PDF of the convergence field  $\kappa(\theta_0)$ .  $\phi(y)$  exhibits a singularity for small but negative value of  $y_s$

$$\phi(y) = \phi_s - a_s \Gamma(\omega_s)(y - y_s)^{-\omega_s}. \quad (23)$$

The parameter  $k_a$  which we have introduced in the definition of  $\mathcal{G}(\tau)$  can be related to the parameters  $a$  and  $\omega$  appearing in the asymptotic expressions of  $\phi(y)$  (Balian & Schaeffer 1989, Bernardeau & Schaeffer 1992).

$$\omega = k_a / (k_a + 2) \quad (24)$$

$$a = \frac{k_a + 2}{2} k_a^{k_a / (k_a + 2)} \quad (25)$$

Similarly the parameters  $y_s$  and  $a_s$  which describe the behavior of  $\phi(y)$  near the singularity can be related to the behavior of  $\mathcal{G}(\tau)$  near its singularity  $\tau_s$ , which is given by (Balian & Schaeffer 1989, Bernardeau & Schaeffer 1992)

$$\tau_s = \frac{\mathcal{G}'(\tau_s)}{\mathcal{G}''(\tau_s)}. \quad (26)$$

The parameter  $y_s$  can be expressed as (Balian & Schaeffer 1989, Bernardeau & Schaeffer 1992)

$$y_s = -\frac{\tau_s}{\mathcal{G}'(\tau_s)}, \quad (27)$$

which in turn can be related to  $k_a$  as

$$-\frac{1}{y_s} = x_* = \frac{1}{k_a} \frac{(k_a + 2)^{k_a + 2}}{(k_a + 1)^{k_a + 1}}. \quad (28)$$

These singularities describe  $P(\delta)$  for large values of  $\delta$ . The newly introduced variable  $x_*$  will be useful later to define the large  $\delta$  tail of  $P(\delta)$ . The different asymptotes in  $\phi(y)$  are linked to the behavior of  $P(\delta)$  for various values of  $\delta$ . However for very large values of the variance i.e.  $\xi_2^2$  it is possible to define a scaling function  $P(\delta) = h(x)/\xi_2^2$  which will encode the scaling

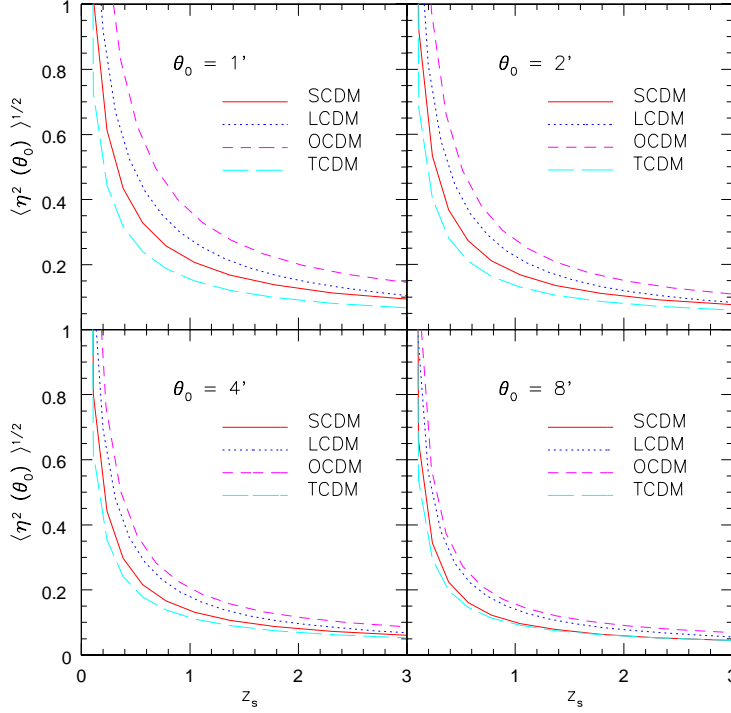


**Figure 1.** Analytical predictions for the variance of the reduced convergence field  $\eta$  as a function of red-shift. Note that whereas the variance of  $\kappa(\theta_0)$  increases with increasing source red-shift, the trend is reversed for  $\eta(\theta_0)$ . Both  $\eta(\theta_0)$  and  $\kappa(\theta_0)$  decrease with increasing smoothing radius  $\theta_0$ .

behavior of the PDF, where  $x$  plays the role of the scaling variable and is defined as  $(1 + \delta)/\xi_2$ . We list the different ranges of  $\delta$  and specify the behavior of  $P(\delta)$  in these regimes (Balian & Schaeffer 1989).

$$\bar{\xi}_2^{\frac{-\omega}{(1-\omega)}} \ll 1 + \delta \ll \bar{\xi}_2; \quad P(\delta) = \frac{a}{\xi_2^2} \frac{1-\omega}{\Gamma(\omega)} \left( \frac{1+\delta}{\xi_2} \right)^{\omega-2} \quad (29)$$

$$1 + \delta \gg \bar{\xi}_2; \quad P(\delta) = \frac{a_s}{\xi_2^2} \left( \frac{1+\delta}{\bar{\xi}_2} \right) \exp \left( - \frac{1+\delta}{x_* \bar{\xi}_2} \right) \quad (30)$$

The integral constraints satisfied by the scaling function are  $S_1 = \int_0^\infty x h(x) dx = 1$  and  $S_2 = \int_0^\infty x^2 h(x) dx = 1$ . These constraints lead to the correct normalization of  $P(\delta)$ . Several numerical studies have been conducted to study the behavior of  $h(x)$  for different initial conditions (e.g. Colombi et al. 1996; Munshi et al. 99). For very small values of  $\delta$  the behavior of  $P(\delta)$  is determined by the asymptotic behavior of  $\phi(y)$  for large values of  $y$ . Hence the PDF can be expressed as (Balian & Schaeffer 1989):

$$P(\delta) = \int_{-i\infty}^{\infty} \frac{dy}{2\pi i} \exp \left[ \frac{(1+\delta)y - ay^{-\omega}}{\bar{\xi}_2} \right]. \quad (31)$$

The above equation implies that it is possible to define another scaling function  $g(z)$ , completely determined by  $\omega$ , with the scaling parameter  $z = (1+\delta)a^{-1/(1-\omega)}\bar{\xi}_2^{\omega/(1-\omega)}$ . However, numerically it is much easier to determine  $\omega$  from the study of  $\sigma(y)$  compared to that from  $g(z)$  (e.g. Bouchet & Hernquist 1992).

$$1 + \delta \ll \bar{\xi}_2; \quad P(\delta) = a^{\frac{-1}{(1-\omega)}} \bar{\xi}_2^{\frac{\omega}{(1-\omega)}} g(z) \quad (32)$$

$$g(z) = \int_{i\infty}^{i\infty} \frac{dt}{2\pi i} \exp(zt - t^{1-\omega}) \quad (33)$$

$$P(\delta) = a^{\frac{-1}{1-\omega}} \bar{\xi}_2^{\frac{\omega}{1-\omega}} \sqrt{\frac{(1-\omega)^{1/\omega}}{2\pi\omega z^{(1+\omega)/\omega}}} \exp \left[ -\omega \left( \frac{z}{1-\omega} \right)^{-\frac{1-\omega}{\omega}} \right] \quad (34)$$

To summarize, the entire behavior of  $P(\delta)$  is encoded in the two scaling functions,  $h(x)$  and  $g(x)$ . These functions are relevant for the behavior of  $P(\delta)$  at small and large  $\delta$ , respectively. Typically  $P(\delta)$  shows a cutoff at both large and small values of  $\delta$  and exhibits a power-law in the middle. The power law behavior is observed when both  $g(z)$  and  $h(x)$  overlap, in the highly

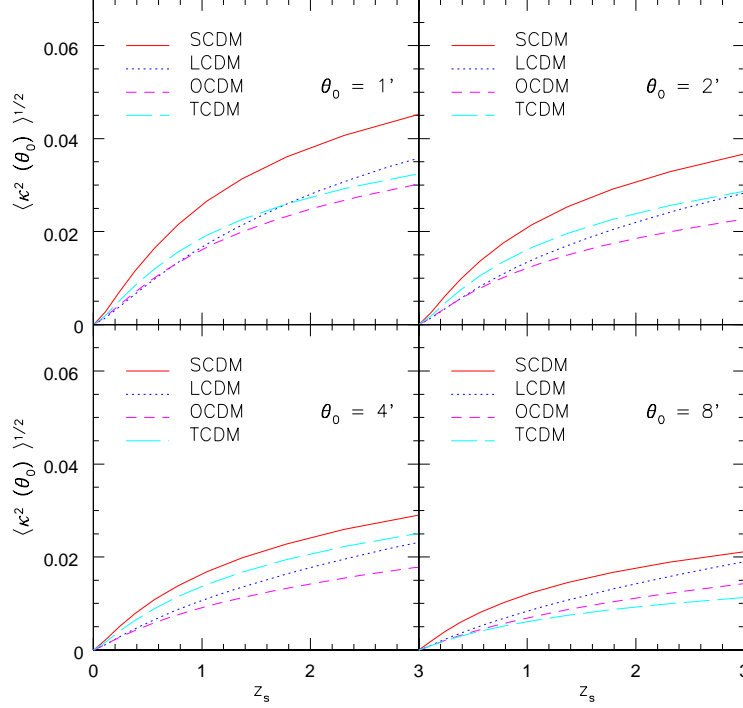


**Figure 2.** The variance of the convergence field  $\langle \kappa^2(\theta_0) \rangle$  as a function of red-shift  $z_s$ . Different panels correspond to different smoothing angles. Note that the ordering of the variance for the convergence field of different cosmological models is not the same as that of the reduced convergence field  $\eta$ .

non-linear regime and with the decrease in  $\bar{\xi}_2$  the range of  $\delta$  for which  $P(\delta)$  shows such a power law behavior decreases, finally to vanish in case of small variance i.e. in the quasi-linear regime.

In the quasi-linear regime exactly the same formalism can be used to study the PDF. However the generating function now can be explicitly evaluated by using tree-level perturbative dynamics (Bernardeau 1992). It is also possible to take smoothing corrections into account in which case one can have an explicit relation of  $\omega$  and the initial power spectral index  $n$ . In general the parameters  $k_a$  or  $\omega$  characterising the VPF or the CPDF are different from their highly non-linear counterparts.

The PDF now can be expressed in terms of  $G_\delta(\tau)$  (Bernardeau 1992, Bernardeau 1994):

$$P(\delta) d\delta = \frac{1}{-G'_\delta(\tau)} \left[ \frac{1 - \tau G''_\delta(\tau)/G'_\delta(\tau)}{2\pi\bar{\xi}_2} \right]^{1/2} \exp\left(-\frac{\tau^2}{2\bar{\xi}_2}\right) d\tau \quad (35)$$

$$G_\delta(\tau) = \mathcal{G}(\tau) - 1 = \delta \quad (36)$$

The above expression for  $P(\delta)$  is valid for  $\delta < \delta_c$  where  $\delta_c$  is the value of  $\delta$  which cancels the numerator of the prefactor of the exponential function appearing in the above expression. For  $\delta > \delta_c$  the PDF develops an exponential tail which is related to the presence of a singularity in  $\phi(y)$ , as was the case of its highly non-linear counterpart (Bernardeau 1992, Bernardeau 1994),

$$P(\delta) d\delta = \frac{3a_s\sqrt{\bar{\xi}_2}}{4\sqrt{\pi}} \delta^{-5/2} \exp\left[-|y_s| \frac{\delta}{\bar{\xi}_2} + \frac{|\phi_s|}{\bar{\xi}_2}\right] d\delta \quad (37)$$

Since the value of the parameter  $\omega$  is different in the two regimes, the associated parameters such as  $y_s$  and  $a_s$  will also be different in these two regimes. We will show that the expressions for the probability distribution function  $P(\eta)$  of the reduced convergence  $\eta$  will have exactly the same asymptotes as the weakly non-linear PDF of  $P(1 + \delta)$ , although the parameters associated with  $P(\eta)$  will correspond to the ones used in the highly non-linear regime for  $P(1 + \delta)$ . This is one of the important result of our analysis.

It may be noted that similar expressions can be derived for the approximate dynamics sometimes used to simulate gravitational clustering in the weakly non-linear regime, e.g. Lagrangian perturbation theory which is an extension of the Zeldovich approximation (Munshi et al. 1994).

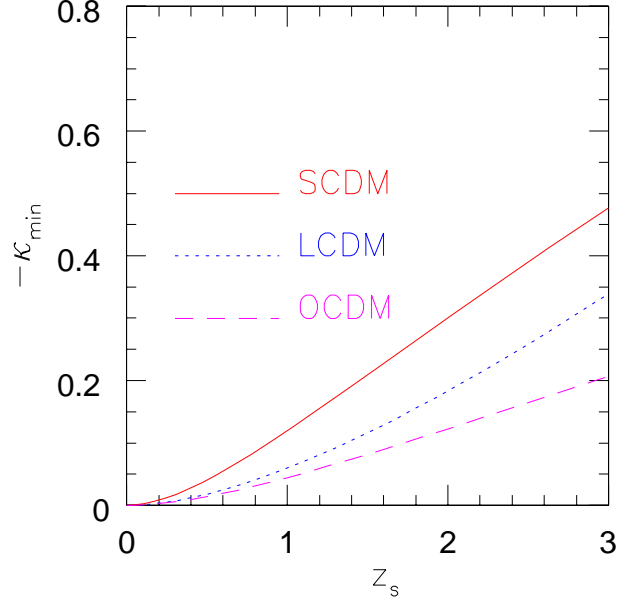


**Figure 3.** The minimum value of  $\kappa(\theta_0)$ , i.e.  $-\kappa_{min}$  is plotted as a function of the source red-shift  $z_s$ . The minimum value of  $\kappa$  occurs in those line of sight direction where smoothed density perturbation  $\delta = -1$  all along the line of sight. It is independent of the smoothing angle  $\theta_0$  and depends only on the background geometry.

### 3.4 PDF of the Smoothed Convergence Field

For computing the probability distribution function of the smoothed convergence field  $\kappa(\theta_0)$ , we will begin by constructing its associated cumulant generating function  $\Phi_{1+\kappa(\theta_0)}(y)$ :

$$\Phi_{1+\kappa(\theta_0)}(y) = y + \sum_{p=2}^{\infty} \frac{\langle \kappa^p(\theta_0) \rangle}{\langle \kappa(\theta_0) \rangle^{p-1}} y^p \quad (38)$$

Now using the expressions for the higher moments of the convergence in terms of the matter power spectrum (equations 6 and 12) gives,

$$\Phi_{1+\kappa(\theta_0)}(y) = y + \int_0^{\chi_s} \sum_{N=2}^{\infty} \frac{(-1)^N}{N!} S_N \frac{\omega^N(\chi)}{r^{2(N-1)}(\chi)} \left[ \int \frac{d^2 \mathbf{l}}{(2\pi)^2} P\left(\frac{l}{r(\chi)}\right) W_2^2(l\theta_0) \right]^{(N-1)} \frac{y^N}{\langle \kappa^2(\theta_0) \rangle^{(N-1)}}. \quad (39)$$

We can now use the definition of  $\phi(y)$  for the matter cumulants to express  $\Phi_{1+\kappa(\theta_0)}(y)$ , in terms of  $\phi(y)$ :

$$\Phi_{1+\kappa(\theta_0)}(y) = \int_0^{\chi_s} d\chi \left[ \frac{\langle r^2(\chi) \kappa_{\theta}^2 \rangle}{\int \frac{d^2 \mathbf{l}}{(2\pi)^2} P\left(\frac{l}{r(\chi)}\right) W_2^2(l\theta_0)} \right] \phi \left[ \frac{\omega(\chi)}{r^2(\chi)} \frac{\int \frac{d^2 \mathbf{l}}{(2\pi)^2} P\left(\frac{l}{r(\chi)}\right) W_2^2(l\theta_0)}{\langle \kappa^2(\theta_0) \rangle} \right] - y \int_0^{\chi_s} \omega(\chi) d\chi \quad (40)$$

The extra term comes from the  $N = 1$  term in the expansion of  $\Phi_{1+\kappa(\theta_0)}$ . Note that we have used the fully non-linear generating function  $\phi$  for the cumulants, though we will use it to construct a generating function in the quasi-linear regime. The analysis becomes much easier if we define a new reduced convergence field  $\eta(\theta_0)$ :

$$\eta(\theta_0) = \frac{\kappa(\theta_0) - \kappa_{min}}{-\kappa_{min}} = 1 + \frac{\kappa(\theta_0)}{|\kappa_{min}|}, \quad (41)$$

where the minimum value of  $\kappa(\theta_0)$  i.e.  $\kappa_{min}$  occurs when the line of sight goes through regions that are completely empty of matter (i.e.  $\delta = -1$  all along the line of sight):

$$\kappa_{min} = - \int_0^{\chi_s} d\chi \omega(\chi). \quad (42)$$

Figures 1 and 2 compare the variance of  $\eta$  and  $\kappa$ . While  $\kappa(\theta_0)$  depends on the smoothing angle, its minimum value  $\kappa_{min}$  depends only on the source red-shift and background geometry of the universe, independent of the smoothing radius. Figure 3 shows the dependence of  $\kappa_{min}$  on source red-shift for three cosmological models. With the reduced convergence  $\eta$ , the cumulant generating function is given by,



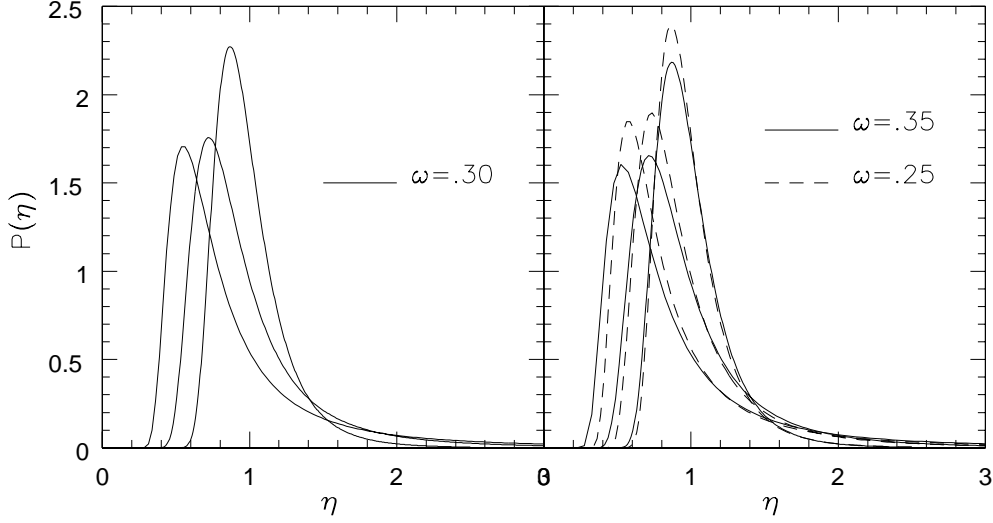


**Figure 4.** Analytical predictions for the probability distribution function  $P(\eta)$  as a function of the reduced convergence  $\eta$ . Curves from left to right correspond to decreasing values of the variance  $\sqrt{\xi_\eta} = .25, .5, \text{ and } 1.$  In all our comparison with ray tracing experiments we have used  $\omega = 0.3$ . However there are some uncertainties in estimation of  $\omega$  from numerical simulations (see Colombi et. al. 1996; Munshi et al. 1999). In the right panel we show how small changes in  $\omega$  change the probability distribution function for the reduced convergence  $\eta$ .

$$\Phi_\eta(y) = \frac{1}{[\int_0^{\chi_s} \omega(\chi) d\chi]} \int_0^{\chi_s} d\chi \left[ \frac{r^2(\chi)}{\int_0^{\chi_s} \omega(\chi) d\chi} \frac{\langle \kappa^2(\theta_0) \rangle}{\int \frac{d^2 \mathbf{l}}{(2\pi)^2} P\left(\frac{l}{r(\chi)}\right) W_2^2(l\theta_0)} \right] \phi \left[ \omega(\chi) \int_0^{\chi_s} \omega(\chi) d\chi \frac{\int \frac{d^2 \mathbf{l}}{(2\pi)^2} P\left(\frac{l}{r(\chi)}\right) W_2^2(l\theta_0)}{r^2(\chi) \langle \kappa^2(\theta_0) \rangle} \right] \quad (43)$$

The constructed cumulant generating function  $\Phi_\eta(y)$  satisfies the normalization constraints  $S_1 = S_2 = 1$ . The scaling function associated with  $P(\eta)$  can now be easily related with the matter scaling function  $h(x)$  introduced earlier:

$$h_\eta(x) = - \int_{-\infty}^{\infty} \frac{dy}{2\pi i} \exp(xy) \Phi_\eta(y). \quad (44)$$

Using this definition we can write:

$$h_\eta(x) = \frac{1}{[\int_0^{\chi_s} d\chi \omega(\chi)]} \int_0^{\chi_s} \omega(\chi) d\chi \left[ \frac{\langle \kappa_{\theta_0}^2 \rangle}{\omega(\chi) \int d^2 \mathbf{k}_\perp P(\mathbf{k}_\perp) W^2(\mathbf{k}_\perp \theta_0 r(\chi)) \int_0^{\chi_s} d\chi \omega(\chi)} \right]^2 \times \quad (45)$$

$$h \left( \frac{\langle \kappa_{\theta_0}^2 \rangle x}{\omega(\chi) \int d^2 \mathbf{k}_\perp P(\mathbf{k}_\perp) W^2(\mathbf{k}_\perp \theta_0 r(\chi)) \int_0^{\chi_s} d\chi \omega(\chi)} \right).$$

While the expressions derived above are exact and are derived for the most general case using only the small angle approximation, they can be simplified considerably using further approximations. In the following we will assume that the contribution to the  $\chi$  integrals can be replaced by an average value coming from the maximum of  $\omega(\chi)$ , i.e.  $\chi_c$  ( $0 < \chi_c < \chi_s$ ). So we replace  $\int f(\chi) d\chi$  by  $1/2 f(\chi_c) \Delta_\chi$  where  $\Delta_\chi$  is the interval of integration, and  $f(\chi)$  is the function of  $\chi$  under consideration. Similarly we replace the  $\omega(\chi)$  dependence in the  $\mathbf{k}$  integrals by  $\omega(\chi_c)$ . Under these approximations we can write,

$$\Phi_\eta(y) = \phi(y) \quad (46)$$

$$h_\eta(x) = h(x) \quad (47)$$

Thus we find that the statistics of the underlying field  $1 + \delta$  and the statistics of the reduced convergence  $\eta$  are exactly the same under such an approximation (the approximate functions  $\Phi_\eta$  and  $h_\eta(x)$  do satisfy the proper normalization constraints). Although it is possible to integrate the exact expressions of the scaling functions, there is some uncertainty involved in the actual determination of these functions and associated parameters such as  $\omega, k_a, x_*$  from N-body simulations (e.g. see Munshi et al. 1999, Valageas et al. 1999 and Colombi et al. 1996 for a detailed description of the effect of the finite volume correction involved in their estimation). We have used  $\Phi_\eta(y)$  as derived above to compute  $P(\eta)$  with the help of equation (21).

An Edgeworth expansion of the pdf can be made by starting with the simpler form  $P(\eta(\theta_0))$ , which can then be used to construct the Edgeworth series for  $P(\kappa(\theta_0))$ . The Edgeworth expansion (see e.g. Bernardeau & Koffman 1994) is meaningful when the variance is less than unity, which guarantees a convergent series expansion in terms of Hermite polynomials  $H_n(\nu)$ ,

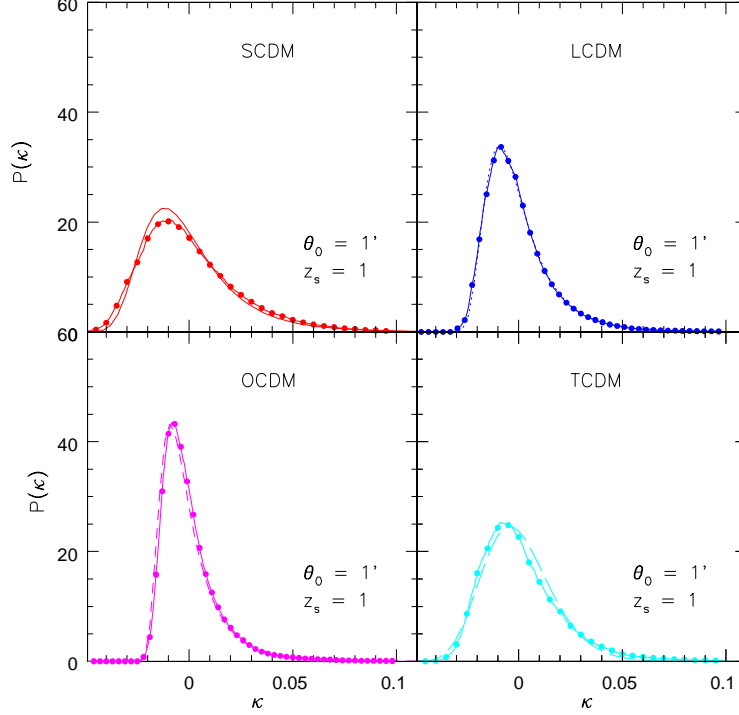


**Figure 5.** Analytical predictions for probability distribution function of the weak lensing convergence field  $P(\kappa)$  smoothed with an angle  $\theta_0 = 1'$  is plotted as a function of  $\kappa$ . The source red-shift is fixed at  $z_s = 1$ . The four curves correspond to the SCDM, LCDM, OCDM and TCDM models as indicated. The Solid lines with black dots are the results from ray tracing simulations.

of order  $n$  and with  $\nu = \eta/\sqrt{(\xi_\eta)}$ . Hence it is used in quasi-linear analysis with the perturbative expressions for cumulants. However the  $S_N^\eta$  parameters used in the expansion of  $P(\eta)$  are from the highly non-linear regime; i.e. although the variance is smaller than unity, the parameters that characterize it are from the highly non-linear dynamics of the underlying dark matter distribution.

$$P(\eta) \equiv \frac{1}{\sqrt{2\pi}\xi_\eta} \exp\left(-\frac{\nu^2}{2}\right) \left[ 1 + \sqrt{\xi_\eta} \frac{S_3^\eta}{6} H_3(\nu) + \sqrt{\xi_\eta}^2 \left( \frac{S_4^\eta}{24} H_4(\nu) + \frac{S_3^{\eta 2}}{72} H_6(\nu) \right) + \dots \right] \quad (48)$$

The magnification  $\mu$  can also be used instead of  $\kappa$  using the weak lensing relation  $\mu(\theta_0) = 1 + 2\kappa(\theta_0)$ . Its minimum value can be related to  $\kappa_{min}$  defined earlier as  $\mu_{min} = 1 + 2\kappa_{min}$ . Finally, the reduced convergence  $\eta$  and the magnification  $\mu$  can be related by the following equation (Valageas 1999):

$$\eta(\theta_0) = \frac{\mu(\theta_0) - \mu_{min}}{1 - \mu_{min}}. \quad (49)$$

So we can express the relations connecting the probability distribution function for the smoothed convergence statistics  $\kappa(\theta_0)$ , the reduced convergence  $\eta(\theta_0)$  and the magnification  $\mu(\theta_0)$  as,

$$P(\kappa(\theta_0)) = 2P(\mu) = P(\eta) \frac{2}{(1 - \mu_{min})} = P(\eta) \frac{1}{|\kappa_{min}|}. \quad (50)$$

Throughout our analysis we have used a top-hat filter for smoothing the convergence field, but our study can be extended to compensated filters (Schneider et al. 1998; Reblinsky et al. 1999), which may be more suitable for observational purposes. The formalism which we have developed for one-point statistics such as the PDF and the VPF can also be extended to compute the bias and higher order cumulants associated with spots in  $\kappa$  maps above a certain threshold. The statistics of such spots can be associated with the statistics of over-dense regions in the underlying mass distribution which represent the collapsed objects. A detailed analysis of these issues will be presented elsewhere (Munshi & Coles 1999b).

#### 4 COMPARISON WITH RAY TRACING SIMULATIONS

To compare analytical results with numerical simulations we smooth the convergence maps generated from numerical simulations using a top-hat filter of suitable smoothing angle  $\theta_0$ . The minimum smoothing radius we have used is  $1'$  which is much larger than the numerical resolution length scale. The maximum smoothing radius we have studied is  $8'$  which is much smaller

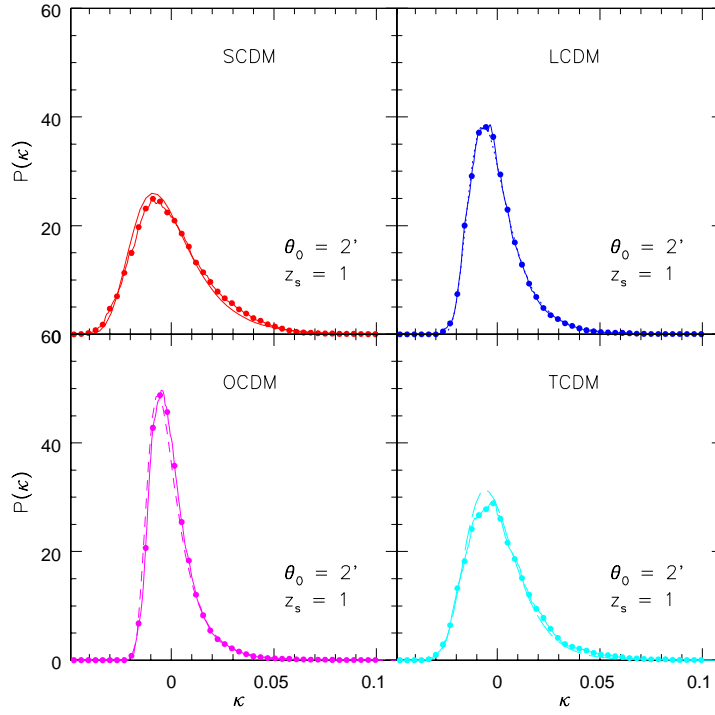


**Figure 6.** As in Figure 5, with smoothing angle  $\theta_0 = 2'$ .

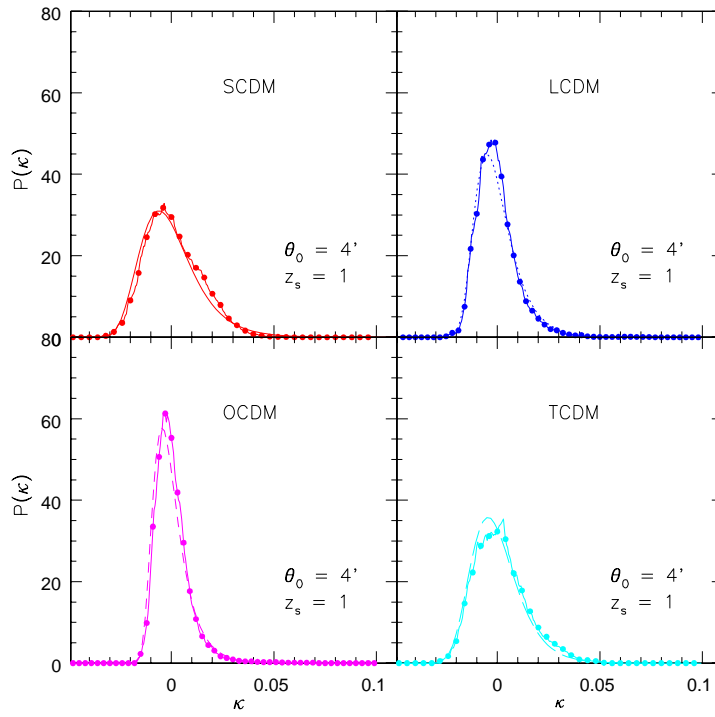


**Figure 7.** As in Figure 5, with smoothing angle  $\theta_0 = 4'$ .

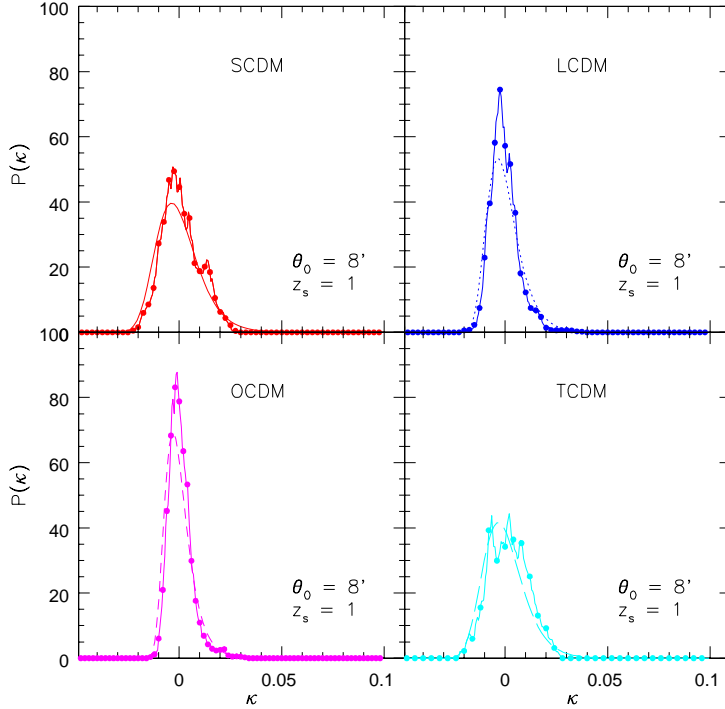


**Figure 8.** As in Figure 5, with smoothing angle  $\theta_0 = 8'$ .

than the box size and we expect that finite volume effects are not significant in our studies. The box size is  $L = 166.28'$  for the EDS models,  $L = 235.68'$  for the  $\Omega = 0.3$  open model, and  $L = 209.44'$  for the  $\Omega = 0.3$  model with cosmological constant  $\Lambda = 0.7$ . Numerical outputs from one realization of each of these cosmological models were used to compare against theoretical results. Elsewhere, we have used these simulations to test analytical results for cumulants and cumulant correlators and found very good agreement.

Figures 4-8 show the analytical and numerical pdf's for the four cosmological models for  $z_s = 1$  and smoothing angles ranging from  $\theta_0 = 1' - 8'$ . Figures 9 and 10 show the dependence on  $z_s$ , by showing the pdf's for  $\theta_0 = 1'$  with  $z_s = 0.5$  and  $z_s = 2$  respectively. Several qualitative features in  $P(\kappa(\theta_0))$  can be understood from the results shown. As we decrease the smoothing angle, the peak of the pdf curves shifts towards negative values of  $\kappa(\theta_0)$ , the peak height decreases and the distribution becomes more non-Gaussian. The reason is that when we decrease the smoothing angle we probe more non-linear scales in the underlying mass distribution and therefore the probability distribution for  $\kappa(\theta_0)$  is more non-linear. Increasing the source red-shift  $z_s$  has two distinct effects. It introduces more dark matter regions between the observer and the source which are virtually uncorrelated with each other. This has the effect of making probability distribution more Gaussian, even though the variance increases due to the increased path length. The peak height of the PDF decreases with increasing red-shift  $z_s$  and  $P(\kappa(\theta_0))$  becomes broader with the increase in the variance.

For given smoothing angle and fixed redshift, the PDFs of the OCDM model are peaked most sharply, followed by that of the LCDM, TCDM and SCDM models. With the reduced convergence field  $\eta(\theta_0)$ ,  $P(\eta(\theta_0))$  does not depend on the background geometry of the universe. We have noted that due to the presence of an extra  $|\kappa_{min}|$  in the denominator, the variance of the reduced convergence  $\eta$  actually decreases with red-shift  $z_s$  in contrast to the variance of  $\kappa(\theta_0)$ . The skewness and other higher order moments for  $\eta$  are also the same as for underlying mass distribution  $\delta$ . It is therefore easy to understand that the PDF of the  $\eta$  field is independent of background cosmological parameters and is very similar to the PDF of the density contrast  $\delta$ . However the difference is that variance of  $\delta$  is much larger than unity, while that of  $\eta$  is much smaller than unity, although the moments and hence the VPF associated with them are exactly the same. The cosmological dependence of  $P(\kappa)$  enters through  $\kappa_{min}$  and  $\langle \eta^2(\theta_0) \rangle$ . Since  $P(\eta(\theta_0))/|\kappa_{min}| = P(\kappa(\theta_0))$ , the peak height of  $P(\eta)$  is determined by the relative ordering of  $|\kappa_{min}|$ , for given red-shift. Thus we find that  $|\kappa_{min}|$  and  $\langle \eta^2(\theta_0) \rangle$  play a very important role in the construction of  $P(\kappa(\theta_0))$ .

The approximation we have used to simplify the void probability distribution function of  $\eta$  also gives us simple and new powerful method to compute the  $S_N$  parameters for the convergence field, by relating them with with the  $S_N$  parameters of the underlying mass distribution as  $S_N^{wl} = S_N / (|\kappa_{min}|)^{N-2}$ .

The comparison of the analytical results with numerical simulations shown in figures 4-8 shows that there is a very good match, particularly for small smoothing angles. The exponential tail for positive values of  $\kappa$  is well reproduced by our analytical results. The analytical PDF also reproduces correctly the exact position of the maxima and the sharp fall of the PDF for negative values of  $\kappa$ . The relative ordering of the peaks for various cosmological models are also well reproduced.

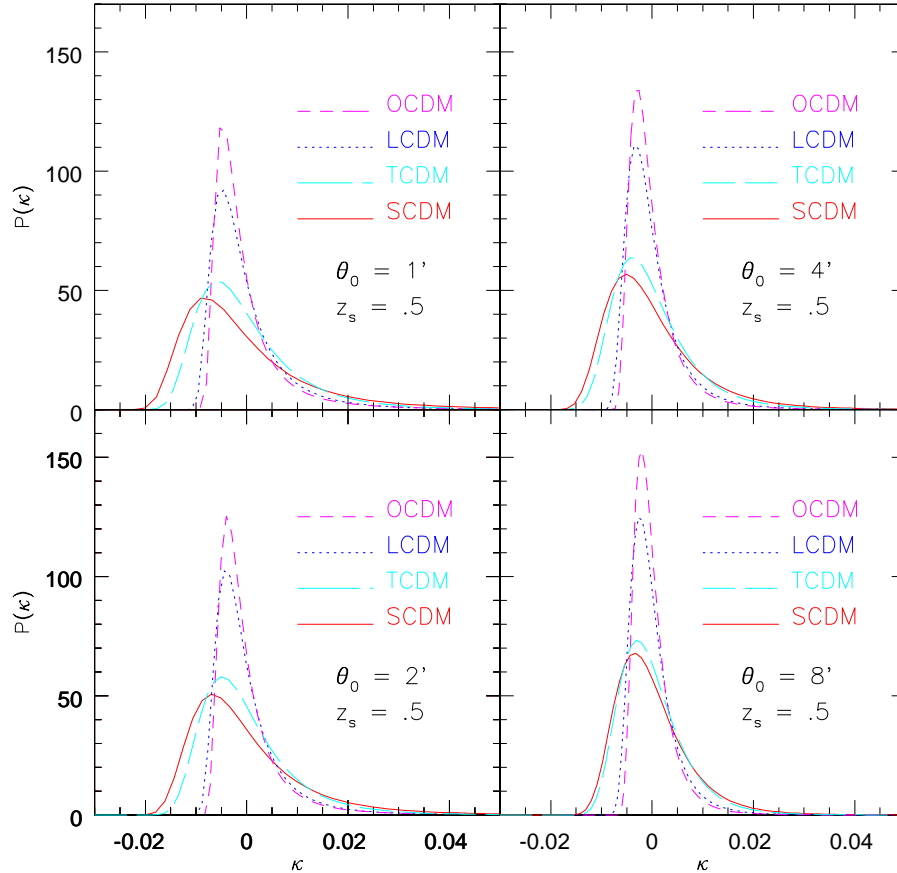


**Figure 9.** Analytical predictions for the probability distribution function  $P(\kappa)$ , smoothed with angle  $\theta_0$ , as a function of  $\kappa$ . The smoothing angle varies from  $1'$  to  $8'$ . The source red-shift is fixed at  $z_s = 0.5$ . The curves with increasing peak heights correspond to the SCDM, LCDM, OCDM and TCDM models.

For large smoothing angles there is some disagreement between the analytical predictions and the ray tracing experiments. This is partially due to the fact that local initial spectral index for length scales making the dominant contribution for larger smoothing angles is different compared to that for the case of small smoothing angle. We have chosen  $\omega = 0.3$  for all our theoretical models, which correspond to initial power spectral index of  $n = -2$ .

For larger smoothing angles length scales contributions to the one-point statistics of the convergence field come from quasi-linear length scales, hence the non-linear theory will not be accurate. In such cases one has to change the generating function  $\mathcal{G}(\tau)$  to the perturbative generating function  $\mathcal{G}^{PT}(\tau)$ . With this change, we can extend all our results in a straight forward way. From the point of view of the Edgeworth expansion, the only change we need to make is in the values of  $S_N$  parameters, where we have to replace the values obtained from the hyper-extended perturbation theory with ones obtained from the tree-level perturbation theory. However for very large smoothing angles ( $\theta_0 > 1^\circ$ ) we have to keep in mind that the small angle approximation is a necessary ingredient in all our analytic calculations.

## 5 DISCUSSION

We have found an analytic expression for the PDF  $P(\kappa(\theta_0))$  of the smoothed convergence field  $\kappa(\theta_0)$ . This is a generalization of our earlier work on lower order cumulants. We found very good agreement of our analytic results with results from ray tracing experiments. We found that the PDF of the convergence field  $\kappa(\theta_0)$  can distinguish different cosmological models. We also show that one can define a reduced convergence field  $\eta(\theta_0)$  which has the same reduced moments as its counterpart for the density contrast  $\delta$ .

While the variance of the convergence increases with source red-shift, the PDF itself tends to become more Gaussian. The differences in PDFs of different cosmological models become less prominent for very large source red-shift. From an observational view point this means that while the detection of weak lensing is easier from deep red-shift surveys, distinguishing cosmological models is easier when the source red-shift is smaller. We have not included the effect of noise due to intrinsic

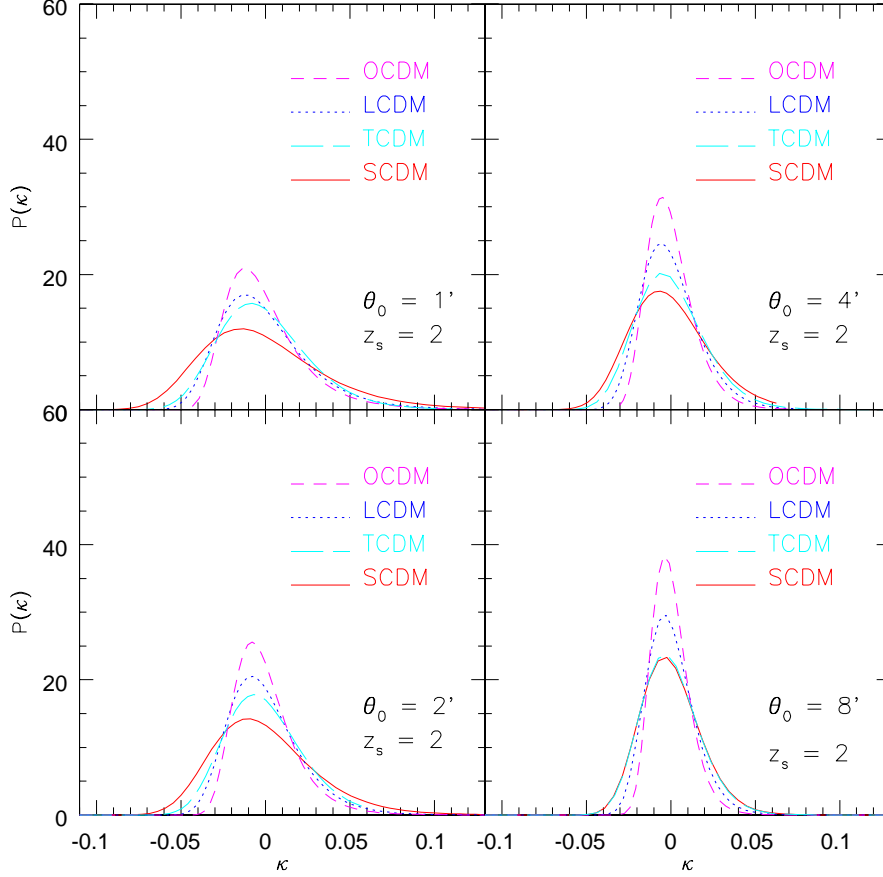


**Figure 10.** As in Figure 9, with source redshift  $z_s = 2$ .

source ellipticity in our calculations. Several authors have focussed on weak gravitational lensing effects in the determination of cosmological parameters from SNeIa observations (e.g. Valageas 1999). Our results match with their finding for small smoothing angles.

The study relating the PDF of the convergence field  $\kappa(\theta_0)$  with the PDF of the density contrast  $\delta$  can be easily extended to relate the  $\kappa_{\theta_0}$  field with the bias associated with high peaks of the density contrast field  $\delta$ . In recent studies (Munshi, Coles & Melott 1999a,b,c; Bernardeau & Scheaffer 1999) it has been shown that the generating function approach used here can be generalized to compute not only the bias associated with the over dense cells but can also provide valuable insight into the statistics of collapsed objects such as cumulants and cumulant correlators. Using the same analytical tools as we have used here, it can be shown that the statistical properties of high  $\kappa(\theta_0)$  spots in convergence maps, e.g. cumulants and cumulant correlators associated with them, can also be related to their counterpart for the density field  $\delta$ . A detailed analysis of the signal to noise ratio is needed to determine the feasibility of estimating these quantities from observational data.

The analytical expression for  $\kappa$  used in this work is a line of sight integration of the density field  $\delta$  which relies on the Born approximation, i.e. it neglects higher order correction terms in the photon propagation equation. The error introduced by such an approximation in the quasi-linear regime has been studied by several authors (e.g. Schneider et al (1997)). Perturbative calculations tend to show that this error is negligible for lower order cumulants, clearly such an analysis is not possible in the highly non linear regime. However since the tail of  $P(\kappa(\theta_0))$  contains information on all orders, a good match between theoretical predictions and the simulation results found by our study indicate that such corrections are negligible even in the highly non-linear regime.

## ACKNOWLEDGMENT

Dipak Munshi was supported by a fellowship from the Humboldt foundation at MPA where this work was completed. It is a pleasure for Dipak Munshi to acknowledge many helpful discussions with Patrick Valageas, Peter Coles and Katrin Reblinsky. The complex integration routine used to generate  $P(\eta)$  was made available to us by Francis Bernardeau; we are grateful to him for his help.

## REFERENCES

- Babul, A., & Lee, M.H., 1991, MNRAS, 250, 407  
Balian R., Schaeffer R., 1989, A& A, 220, 1  
Bartelmann M., Huss H., Colberg J.M., Jenkins A.  
Bartelmann, M. & Schneider, P., 1991, A& A, 248, 353  
Pearce F.R., 1998, A&A, 330, 1  
Bernardeau F., 1992, ApJ, 392, 1  
Bernardeau F., 1999, astro-ph/9901117  
Bernardeau F., Schaeffer R., 1992, A& A, 255, 1  
Bernardeau F., Schaeffer R., 1999, astro-ph/9903087  
Bernardeau F., van Waerbeke L., Mellier Y., 1997, A& A, 322, 1  
Blandford R.D., Saust A.B., Brainerd T.G., Villumsen J.V., 1991, MNRAS, 251, 600  
Boschan P., Szapudi I., Szalay A.S., 1994, ApJS, 93, 65  
Bouchet F.R., & Hernquist, L., 1992, ApJ, 400, 25  
Couchman H.M.P., Barber A.J., Thomas P.A., 1998, astro-ph/9810063  
Davis M., Peebles P.J.E., 1977, ApJS, 34, 425  
Diaferio A., Kauffmann G, Colberg J.M., White S.D.M, 1999, MNRAS, 307, 537  
Fry, J.N., 1984, ApJ, 279, 499  
Fry, J.N., & Peebles, P.J.E., 1978, ApJ, 221, 19  
Groth, E., & Peebles, P.J.E., 1977, ApJ, 217, 385  
Gunn, J.E., 1967, ApJ, 147, 61  
Hamilton A.J.S., Kumar, P., Lu, E. & Matthews, A., 1991, ApJ, 374, L1  
Hui, L., astro-ph/9902275  
Hui, L., & Gaztanaga, astro-ph/9810194  
Jain, B., Mo H.J., & White S.D.M., 1995, MNRAS, 276, L25  
Jain, B., & Seljak, U., 1997, ApJ, 484, 560  
Jain, B., Seljak, U., White, S.D.M., 1999a, astro-ph/9901191  
Jain, B., Seljak, U., White, S.D.M., 1999b, astro-ph/9901287  
Jaroszyn'ski, M., Park, C., Paczynski, B., & Gott, J.R., 1990, ApJ, 365, 22  
Jaroszyn'ski, M. 1991, MNRAS, 249, 430  
Kaiser, N., 1992, ApJ, 388, 272  
Kaiser, N., 1998, ApJ, 498, 26  
Kauffmann G, Colberg J.M., Diaferio A., White S.D.M, 1999a, MNRAS, 303, 188  
Kauffmann G, Colberg J.M., Diaferio A., White S.D.M, 1999b, MNRAS, 307, 529  
Limber D.N., 1954, ApJ, 119, 665  
Lee, M.H., & Paczyn'ski B., 1990, ApJ, 357, 32  
Miralda-Escudé J., 1991, ApJ, 380, 1  
Munshi D., Bernardeau F., Melott A.L., Schaeffer R., 1999, MNRAS, 303, 433  
Munshi D., Melott A.L, 1998, astro-ph/9801011  
Munshi D., Coles P., Melott A.L., 1999a, MNRAS, in press, astro-ph/9812337  
Munshi D., Coles P., Melott A.L., 1999b, MNRAS, in press, astro-ph/9902215  
Munshi D., Melott A.L., Coles P., 1999c, MNRAS, in press, astro-ph/9812271  
Munshi D. & , Coles P., 1999a, MNRAS, in press  
Munshi D. & , Coles P., 1999b, MNRAS, submitted  
Munshi D. & , Jain B., 1999a, MNRAS, submitted  
Mellier Y., 1999, astro-ph/9901116  
Nityananda R., & Padamanabhan T., 1994, MNRAS, 271, 976  
Padmanabhan T., Cen R., Ostriker J.P., Summers, F.J., 1996, ApJ, 466, 604  
Premadi P., Martel H., Matzner R., 1998, ApJ, 493, 10  
Press, W.H., & Schechter, P. 1974, ApJ, 187, 425  
Peebles P.J.E., 1980, *The Large Scale Structure of the Universe*. Princeton University Press, Princeton  
Reblinsky, K., Kruse, G., Jain, B., Schneider, P., astro-ph/9907250  
Schneider, P., & Weiss, A., 1988, ApJ, 330,1  
Schneider, P., van Waerbeke, L., Jain, B. & Kruse, G. 1998, MNRAS, 296, 873, 873  
Scoccimarro R., Colombi S., Fry J.N., Frieman J.A., Hivon E., Melott A.L., 1998, ApJ, 496, 586  
Scoccimarro R., Frieman J., 1998, preprint, astro-ph/9811184  
Szapudi I., Colombi S., 1996, ApJ, 470, 131  
Szapudi I., Szalay A.S., 1993, ApJ, 408, 43  
Szapudi I., Szalay A.S., 1997, ApJ, 481, L1  
Szapudi I., Szalay A.S., Boschan P., 1992, ApJ, 390, 350  
Valageas, P., 1999, astro-ph/9904300  
Valageas, P., Lacey C., Schaeffer R. 1999, astro-ph/9902320  
Valageas, P., Schaeffer R 1997, astro-ph/9710128  
van Waerbeke, L., Bernardeau, F., Mellier, Y., 1998, astro-ph/9807007  
Wambsganss, J., Cen, R., & Ostriker, J.P., 1998, ApJ, 494, 298  
Wambsganss, J., Cen, R., Xu, G. & Ostriker, J.P., 1997, ApJ, 494, 29  
Wambsganss, J., Cen, R., Ostriker, J.P. & Turner, E.L., 1995, Science, 268, 274  
Wang Y., 1999, ApJ, in press.

White, M. & Hu, W., astro-ph/9909165  
White S.D.M, 1979, MNRAS, 186, 145